Calibration and Calculation of Polarization Lidar

Jinhong Xian[1] [ID], **Dongsong Sun[1], Wenjing Xu[2], Chongguo Tian[3,4]** [ID]**, Qingzhi Tan[2], Yuli Han[1], and Shaochen Yang[2]**

[1]School of Earth and Space Sciences, University of Science and Technology of China, Hefei, China, [2]Darsunlaser Technology Co., Ltd., Shenzhen, China, [3]CAS Key Laboratory of Coastal Zone Environmental Processes and Ecological Remediation, Yantai, China, [4]Institute of Coastal Zone Research, Chinese Academy of Sciences, Yantai, China

Abstract Although polarization lidar technology has been widely used to detect depolarized particles, many difficulties still exist in measuring accurate values for the depolarization ratio. This ratio is basically related to the difference between the optical and the electronic gain of the lidar's channels, the polarization purity of the laser pulse, and the error in the alignment between the laser's polarization plane and the polarizer. We propose here an algorithm for the calibration and calculation of polarization lidars. Numerical simulations showed that the depolarization ratio profile retrieved from the proposed algorithm agrees well with the simulated profile. The proposed algorithm no longer requires the laser source to be linearly polarized. Instead, the light polarization can be elliptical or random. During the installation process, the polarization of the detector is no longer required to be parallel or perpendicular to the polarization direction of the laser source and can be done in any direction.

1. Introduction

The measurement of depolarization ratio by polarization lidar provides a useful means for detecting non-spherical mineral dust particles, distinguishing water from ice clouds, and studying the characteristics of ice clouds (Ansmann et al., 2003; Murayama et al., 1999; Sassen 1991; Shimizu et al., 2004; Scotland et al., 1971). The general concept includes two receiving channels for detecting the backscattered light parallel and perpendicular (cross) to the polarization direction of the linearly polarized laser source. This technique is sensitive to the shape of backscattering particles: spherical particles reflect light in the opposite (180°) backscattering direction without changing the polarization, while nonspherical particles reflect light according to their shape, size, and composition (Platt et al., 1987; Sassen et al., 1989). Therefore, polarization lidars can distinguish different types of particles in the atmosphere and are very sensitive to detecting layers containing aspheric particles, such as cirrus clouds or some types of polar stratospheric clouds (Browell et al., 1990).

In spite of the wide use of polarization lidar technology for detecting depolarized particles, many difficulties in measuring the accurate value of the depolarization ratio still remain (Behrendt & Nakamura, 2002; Belegante et al., 2018). The uncertainty in depolarization measurements from lidars comes from various sources but is mostly related to the difference between the optical and the electronic gain of the lidar's channels, the polarization purity of the laser pulse, and the alignment error between the laser's polarization plane and the polarizer (Behrendt et al., 2002; Bravo-Aranda et al., 2016). The two-parallel and cross-polarization components are separated in the receiver by using a polarization beam splitter cube, but this separation is not perfect. In addition, the polarization splitter may be misaligned with the polarization plane of the transmitted laser beam, and a polarization plane rotation is used for the relative calibration of the two receiving channels. Therefore, an equation necessary to obtain the angle between the polarization plane of the laser and the incident plane of the polarization beam splitter cube is necessary and has been devised (Freudenthaler et al., 2009; Freudenthaler, 2016).

In this paper, we propose an algorithm for the calibration and calculation of polarization lidars, whose purpose is to make lidar results independent of polarization orientation. Section 2 introduces the principle of this technique, while a simulation of lidar parameters in an idealized environment, and comparison with actual data is proposed to validate the algorithm in section 3. A discussion based on empirical experiments and a summary are proposed in sections 4 and 5, respectively.

2. Methodology

The parallel- and cross-polarized components of the total backscattered power can be written as (Klett, 1981)

$$P_{\parallel}(r) = \frac{1}{2}\eta_{\parallel}E_0 c A_r \frac{\beta_{\parallel}(r)\exp\left[-2\int_O^r \sigma(r')dr'\right]}{r^2} = \frac{C_{\parallel}\beta_{\parallel}(r)\exp\left[-2\int_O^r \sigma(r')dr'\right]}{r^2}, \tag{1}$$

and

$$P_{\perp}(r) = \frac{1}{2}\eta_{\perp}E_0 c A_r \frac{\beta_{\parallel}(r)\exp\left[-2\int_O^r \sigma(r')dr'\right]}{r^2} = \frac{C_{\perp}\beta_{\perp}(r)\exp\left[-2\int_O^r \sigma(r')dr'\right]}{r^2}, \tag{2}$$

respectively, where E_0, A_r, and c are the single pulse energy of laser, the receiver diameter, and the velocity of light in vacuum; $\sigma(r)$ is the total extinction coefficient; and η, $\beta(r)$, and C ($\parallel$ and $\perp$, respectively, represent the parallel- and cross-polarized channels) are the detection efficiency, the components of the backscatter coefficient at distance r, and the lidar instrumental constant, respectively.

The ratio of the cross-polarized backscatter coefficient to the parallel-polarized backscatter coefficient is called the linear volume depolarization ratio (Sugimoto & Lee, 2006):

$$\delta(r) = \frac{\beta^{\perp}}{\beta_{\parallel}} = \frac{\gamma P^{\perp}}{P^{\parallel}}, \tag{3}$$

where $\frac{C_{\parallel}}{C_{\perp}} = \gamma$ accounts for the differences in the entire detector channels.

In the following calculation, we also use another definition of the particle depolarization ratio (Sugimotod et al., 2006)

$$\delta'(r) = \frac{\beta^{\perp}}{\beta^{\perp} + \beta_{\parallel}} = \frac{\gamma P^{\perp}}{\gamma P^{\perp} + P^{\parallel}}. \tag{4}$$

The following relationships between $\delta(r)$ and $\delta'(r)$ exist

$$\delta(r) = \frac{\delta'(r)}{1 - \delta'(r)}. \tag{5}$$

Without considering the polarization effect, the backscattered power received in the parallel- and cross-polarized channels are P_p and P_s, respectively. When the laser source is a linearly polarized light, ideally, Ps should be zero. However, during the installation process, the polarization direction of the light source and of the detector cannot be made completely parallel; therefore, Ps is not zero. In addition, in some cases of low purity of linear polarization, Ps is also not 0. The system polarization degree, which is described by R, can be expressed as

$$R = \frac{\gamma P_S}{P_P}. \tag{6}$$

Muller matrices describe the linear interaction between polarized light and an optical system (optical elements or medium). Any input can be represented as a Stokes vector (Freudenthaler, 2016). The total input power I_{in} can be represented by the Stokes vector as

$$\mathbf{I}_{\text{in}} = \begin{pmatrix} P_P + \gamma P_S \\ P_P - \gamma P_S \\ m \\ 0 \end{pmatrix}, \tag{7}$$

where $P_P + \gamma P_S$ is related to the laser energy and the parameter m describes different system polarization degrees.

Muller matrix F is used to describe the scattering matrix for randomly oriented particles and can be written as (Freudenthaler, 2016)

$$\mathbf{F} = F_{11} \begin{pmatrix} 1 & 0 & 0 & 0 \\ 0 & a & 0 & 0 \\ 0 & 0 & -a & 0 \\ 0 & 0 & 0 & 1-2a \end{pmatrix}, \tag{8}$$

where F_{11} is the backscatter coefficient and a is the polarization parameter. Both F_{11} and a are range-dependent, and the linear volume depolarization ratio is written as (Freudenthaler, 2016)

$$\delta = \frac{1-a}{1+a} \Rightarrow a = 1-2\delta'. \tag{9}$$

A polarizing splitter separates the received signals into reflection (cross-polarized components) and transmission (parallel-polarized components) signals. Consequently, the reflection (M_S) and transmission (M_P) processes are expressed as

$$\mathbf{M}_S = \frac{1}{2} \begin{pmatrix} 1 & -1 & 0 & 0 \\ -1 & 1 & 0 & 0 \\ 0 & 0 & 0 & 0 \\ 0 & 0 & 0 & 0 \end{pmatrix}, \tag{10}$$

$$\mathbf{M}_P = \frac{1}{2} \begin{pmatrix} 1 & 1 & 0 & 0 \\ 1 & 1 & 0 & 0 \\ 0 & 0 & 0 & 0 \\ 0 & 0 & 0 & 0 \end{pmatrix} \tag{11}$$

respectively.

According to the Stokes-Muller formalism, the reflected signal $\mathbf{P}_\perp$ and the transmitted signal $\mathbf{P}_\parallel$ can be obtained by multiplying the laser beam Stokes vector (I_{in}) by the Muller matrix F, that is,

$$\mathbf{P}_\perp = C_\perp \mathbf{M}_S \mathbf{F} \mathbf{I}_{in} = C_\perp F_{11} \begin{pmatrix} \frac{(1-a)}{2} P_P + \frac{(1+a)}{2} \gamma P_S \\ \frac{(a-1)}{2} P_P - \frac{(1+a)}{2} \gamma P_S \\ 0 \\ 0 \end{pmatrix}, \tag{12}$$

$$\mathbf{P}_\parallel = C_\parallel \mathbf{M}_P \mathbf{F} \mathbf{I}_{in} = C_\parallel F_{11} \begin{pmatrix} \frac{(1+a)}{2} P_P + \frac{(1-a)}{2} \gamma P_S \\ \frac{(a+1)}{2} P_P + \frac{(1-a)}{2} \gamma P_S \\ 0 \\ 0 \end{pmatrix}, \tag{13}$$

respectively.

Thus, the measured signals $P_\perp$ and $P_\parallel$ are

$$P_\perp = C_\perp F_{11} \left[\frac{(1-a)}{2} P_P + \frac{(1+a)}{2} \gamma P \right], \tag{14}$$

$$P_\parallel = C_\parallel F_{11} \left[\frac{(1+a)}{2} P_P + \frac{(1-a)}{2} \gamma P_S \right], \tag{15}$$
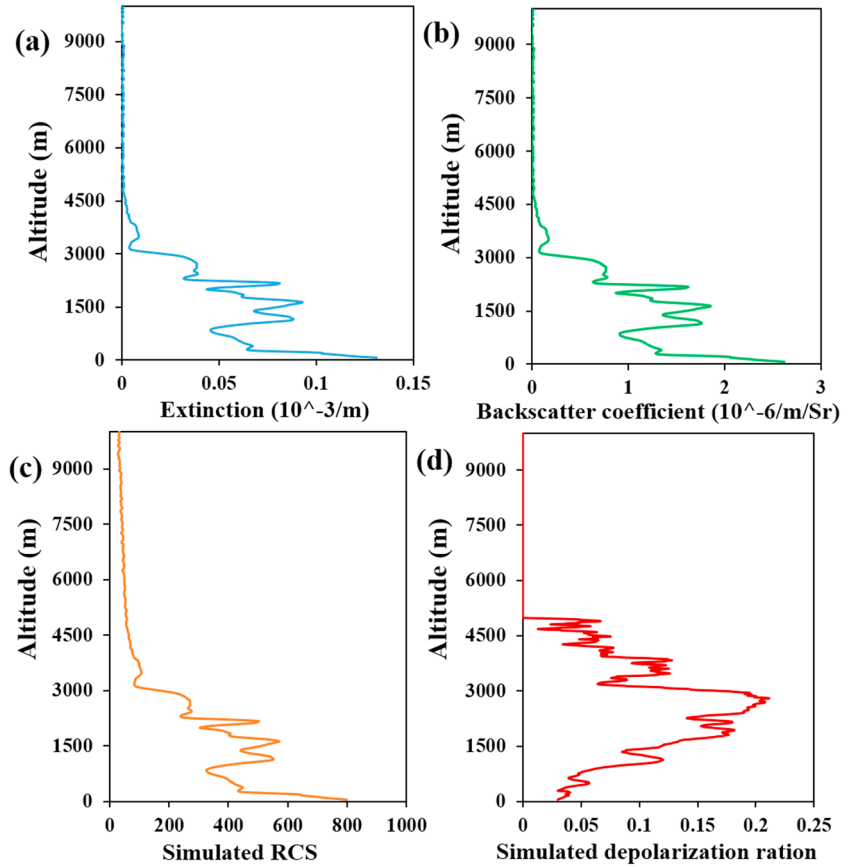
respectively.

Figure 1. (a) Total extinction coefficient, (b) backscatter coefficient, (c) simulated lidar range corrected signal (*RCS*), and (d) simulated depolarization ratio δ(*r*) as a function of altitude.

Substitute equation (9) into equations (14) and (15), The cross- and parallel-polarized components of the total backscattered power are written as

$$P_\perp = C_\perp F_{11}[\gamma P_S(1-\delta') + \delta' P_P],$$
(16)

$$P_\parallel = C_\parallel F_{11}[P_P(1-\delta') + \delta' P_S \gamma],$$
(17)

respectively.

Therefore, the ratio of equations (16) and (17) implies

$$\frac{P_\perp}{P_\parallel} = \frac{C_\perp F_{11}[\gamma P_S(1-\delta') + \delta' P_P)]}{C_\parallel F_{11}[P_P(1-\delta') + \delta' P_S \gamma],}$$
(18)

and the depolarization ratio δ' can be calculated as

$$\delta' = \frac{1 - \frac{\gamma P_\perp}{R P_\parallel}}{\left(1 + \frac{\gamma P_\perp}{P_\parallel}\right)\left(1 - \frac{1}{R}\right)}.$$
(19)

This formula is more general than that described in equation (4). It allows for the depolarization ratio to be calculated under different polarization states and eliminates the errors caused by the nonparallel polarization of the light source and detector during the installation process. From this formula, we can see that *R* cannot equal 1, which means that the laser source can be any kind of polarized light except circularly polarized light.
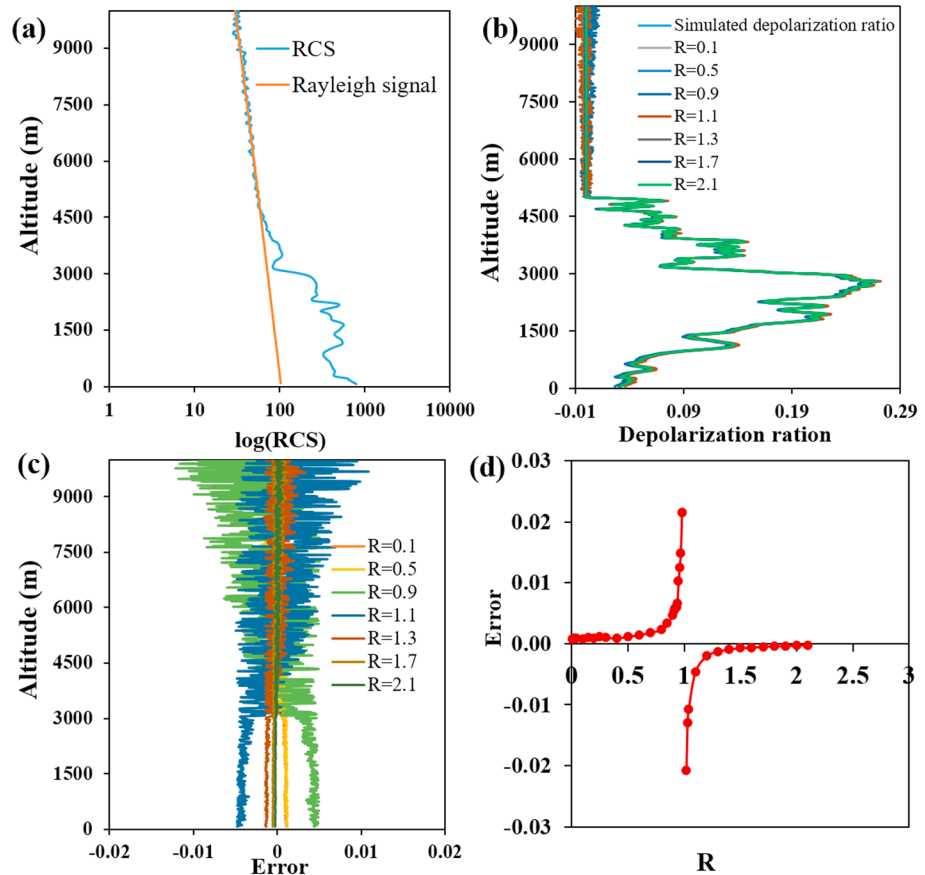
Figure 2. (a) Simulated lidar range corrected signal (*RCS*) fitted to the Rayleigh signal profile, (b) simulated and calculated depolarization ratio for different values of polarization purity *R*, (c) error between simulated and calculated depolarization ratios (for given *R* values), and (d) mean absolute error as a function of *R*.

The system polarization degree *R* can be estimated by monitoring the δ values in the middle and upper troposphere, where the effects of aerosols on depolarization are usually small. For determining this value, a previous study delineated the properties of atmospheric backscatter signals relevant for calculating the molecular depolarization ratio (depending on the receiver bandwidth of a lidar system) (Behrendt et al., 2002). According to this research work, the molecule depolarization ratio is $\delta_{mol} = 0.00363$ (Behrendt et al., 2002). Since the molecule depolarization ratio is not the object of our study, the molecule depolarization ratio is set to 0 here. The amount of error this assumption brings to the aerosol depolarization ratio estimation will be analyzed later.

Molecular extinction coefficient $\sigma_m(r)$ and backscatter coefficient $\beta_m(r)$ can be got from a standard atmospheric model (U.S. Standard Atmosphere). We substitute $\sigma_m(r)$ and $\beta_m(r)$ into equation (1) to obtain Rayleigh signal. In order to find the range where we assume clean air without aerosols, the measured signals are first fitted to the Rayleigh signal profile in the aerosol-free middle-to-upper troposphere (Rayleigh-fit) (Bockmann et al., 2004). The Rayleigh-fit is a normalization of the range corrected lidar signal to the

Table 1
Statistics of Mean Relative Errors Between Simulated and Calculated Depolarization Ratio for Different Values of R

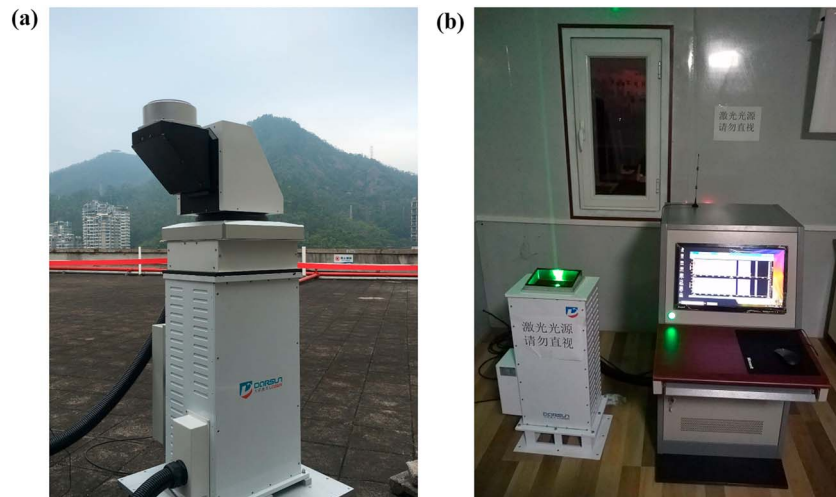| System polarization degree	0.01	0.2	0.4	0.6	0.8	0.9	0.95	0.98	1.02	1.04	1.1	1.2	1.3	1.6	1.8	2
Mean relative error (%)	2.46	2.88	2.86	4.45	7.42	15.00	33.28	69.35	67.23	34.45	14.71	6.47	4.28	2.13	1.36	0.88

Figure 3. Polarization lidar installation at the (a) Shenzhen and (b) Yantai stations.

calculated attenuated molecular backscatter coefficient in a range where the calculated signal fits the lidar signal sufficiently good. The corresponding depolarization ratio was set to zero for the molecular signal or the Rayleigh signal. Therefore, from equation (19), R can be calculated as

$$R = \frac{\gamma P_\perp^{ry}}{P_\parallel^{ry}},$$
(20)

with $P_\parallel^{ry}$ and $P_\perp^{ry}$ as the parallel- and the cross-polarized molecular signals, respectively.

In summary, we can fit the measured signals to the Rayleigh signal profile to find the range where we assume clean air without aerosols and calculate the system polarization degree R, then substitute R into equations (19) and (5) to obtain the depolarization ratio. It can eliminate the errors caused by the nonparallel polarization of the light source and detector during the installation process. From equation (19), we can see that R cannot equal 1. Therefore, the proposed algorithm does no longer require the laser source to be linearly polarized, as elliptical polarized or randomly polarized light (except circular) can be used.
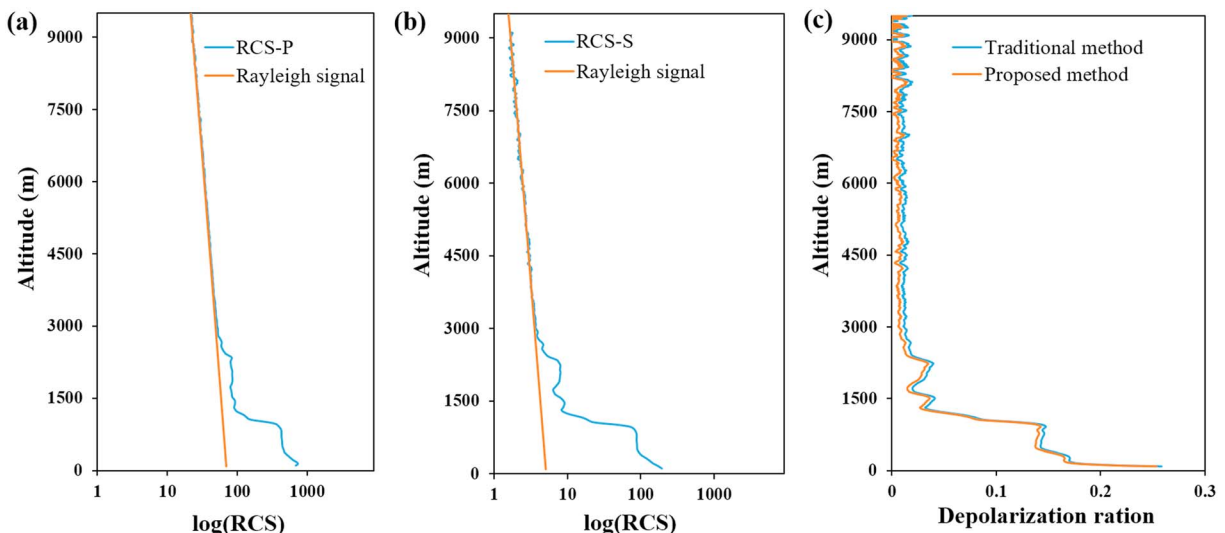

Figure 4. Lidar range corrected signal for the (a) parallel- (*RCS-P*), (b) cross-polarized (*RCS-S*) channel, and (c) depolarization ratio calculated by the traditional and proposed methods at the Shenzhen lidar station on 18 December 2018.
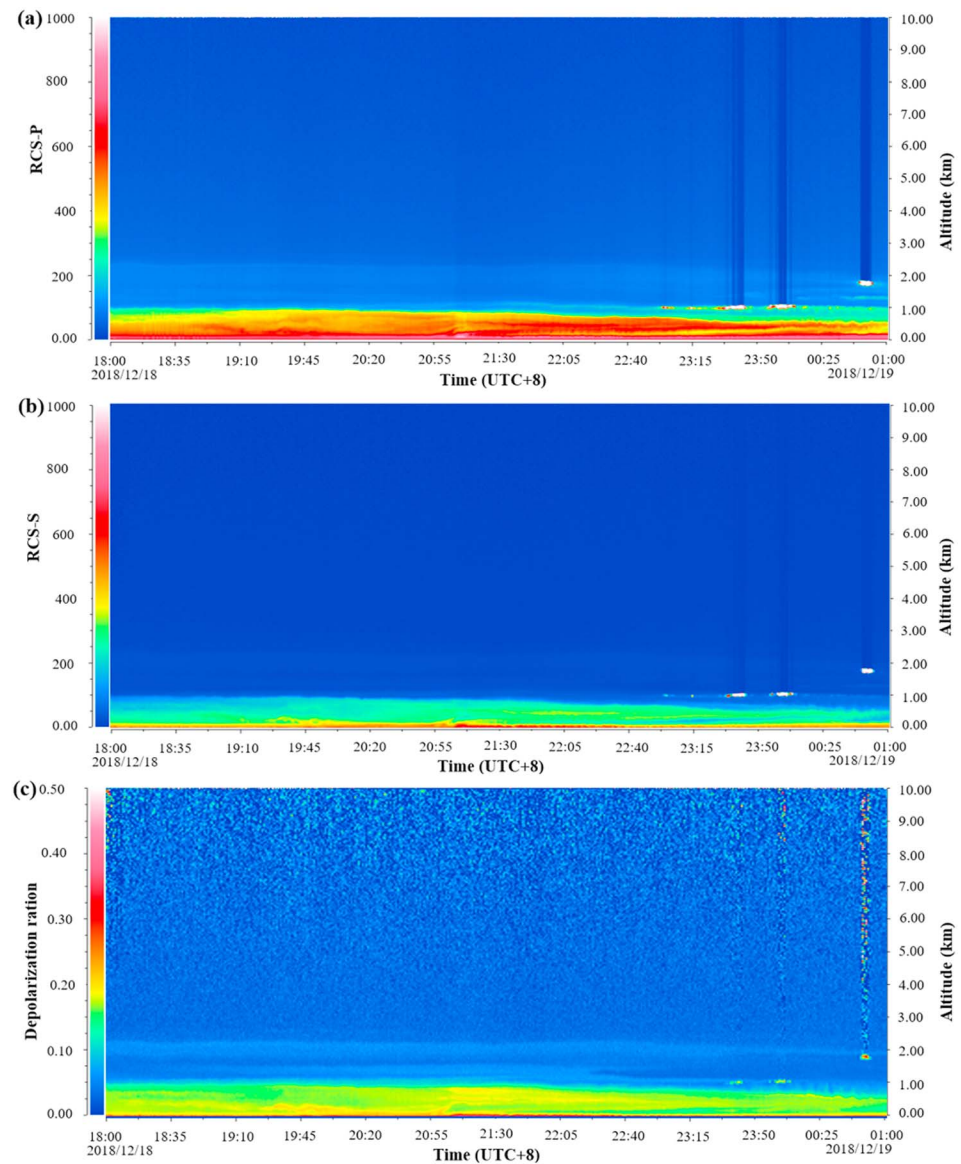
Figure 5. Time-height cross sections of (a) *RCS-P*, (b) *RCS-S*, and (c) depolarization ratio obtained from the proposed algorithm for the lidar data acquired at the Shenzhen station from 18 to 19 December 2018.

3. Numerical Analysis

To verify the proposed algorithm accuracy, we first simulate the range corrected signal (*RCS*). It is assumed that the detection efficiency of both channels ($\eta_{\parallel}$ and $\eta_{\perp}$) is equal to 1. The receiver diameter is set to 100 cm, and the single laser pulse energy of laser is set to 100 μJ. So for given $\sigma(r)$ and $\beta(r)$, as shown in Figures 1a and 1b, we substitute them into equations (1) and (2) to obtain *RCS* (Xian et al., 2018), as shown in Figure 1c. Figure 1d shows the given depolarization ratio $\delta(r)$. At altitudes of 5 km and above, the molecular signal dominates, whereas the level of aerosol concentration is almost 0, and the depolarization ratio is set to 0.00363 (Behrendt et al., 2002). The simulated lidar was set to a horizontal resolution of 15 m and a laser central wavelength of 532 nm, although the algorithm is wavelength independent. To verify the accuracy of the algorithm, while considering different laser pulse polarization purity and different alignments between the polarization plane of the laser and the detector, we set a series of *R* to simulate the *RCS-P* (RCS in the parallel-polarized channel) and the *RCS-S* (RCS in the cross-polarized channel). For a given *RCS-P* and under Poisson noise condition, we set a series of *R* to calculate *RCS-S*. The values *RCS-P*, *RCS-S*, and $\delta(r)$
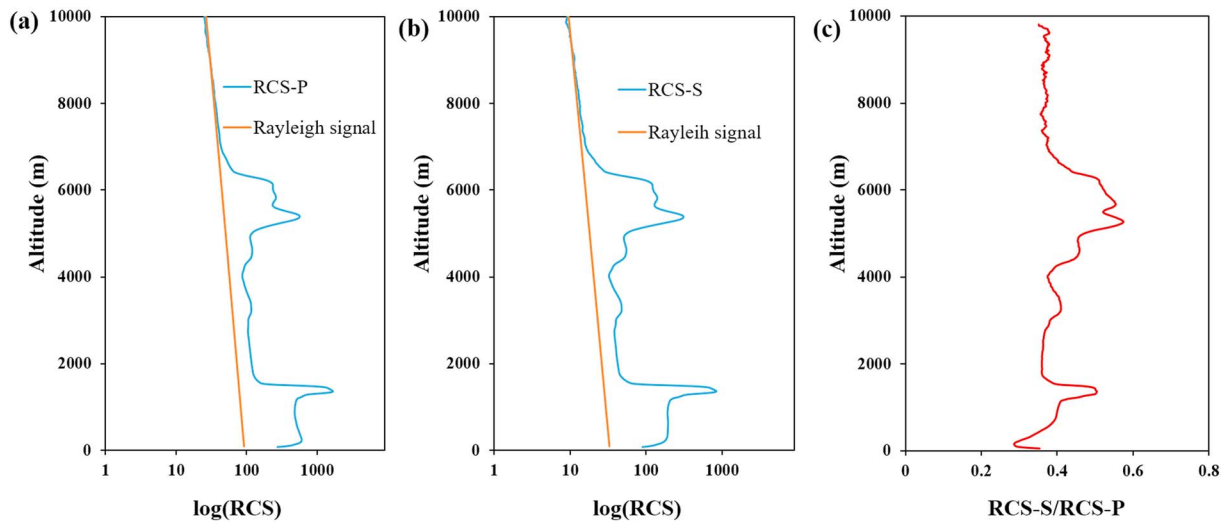
Figure 6. Lidar range corrected signal for the (a) parallel- (*RCS-P*), (b) cross-polarized (*RCS-S*) channel, and (c) the ratio of two channel signals at the Yantai lidar station on 05 December 2018.

are then substituted in equations (16) and (17) to obtain the backscattered power received in the cross- and parallel-polarized channels.

The proposed algorithm is used to solve the simulated signal and obtain the depolarization ratio $\delta(r)$ profile. No data filtering was applied for retrieving the depolarization ratio. Figure 2a shows the fitting of *RCS* with the Rayleigh signal. For different values of *RCS-P* and *RCS-S*, and by fitting the signals of the two channels with the Rayleigh signal at altitudes of 8-10 km, the system polarization degree *R* is calculated. Then, using equations (19) and (5), the depolarization ratio is estimated and compared with the simulated depolarization ratio, as shown in Figure 2b. It can be seen from this figure that the solution obtained is in good agreement with the simulated depolarization ratio. We subtract the calculated results with different *R* from the simulated depolarization ratio and get error curves for each *R* value, as shown in Figure 2c. Due to the Poisson noise at altitudes of 8-10 km, the value of *R* calculated by equation (20) has a range of errors. For different values of *R*, the mean absolute error is obtained by averaging the error of the aerosol depolarization ratio within the first 5 km, as shown in Figure 2d. It can be seen from the figure that for *R* values less than 1, there is a positive average error and for *R* values greater than 1, the average error is negative.

Table 1 summarizes the mean relative error between simulated and calculated depolarization ratio for different values of *R*. When *R* is less than 0.8 or more than 1.2, the mean relative error is less than 5%. From equation (19), we can see that *R* cannot be equal to 1. For values of *R* close to 1, the error is very high, reaching up to 69.35%. Therefore, in actual measurements, *R* should be kept as far away as possible from 1. Compared to uncertainties, which are typically in the range of 5–10 % in the retrieval products discussed by Mamouri et al. (Mamouri et al., 2013), the algorithm proposed in the current study yields lower uncertainty.

4. Results and Discussion

To validate the proposed algorithm performance, we performed a series of experiments in December at the Shenzhen (22.498085°N, 113.920647°E) and Yantai (37.472229°N, 121.446365°E) lidar stations, shown in Figures 3a and 3b. The Shenzhen's polarized lidar light source has a very high degree of linear polarization, which can reach 1000:1, while the Yantai's lidar system polarization degree is relatively low, about 100:30. The wavelength of both lasers is 532 nm.

For the polarization lidar in Shenzhen, the two channel signals *RCS-P* and *RCS-S* measuring during cloudless weather conditions were selected and fitted with the Rayleigh signal, as shown in Figures 4a and 4b. Above an altitude of about 1.5 km, the ratio of the two channels is approximately 0.011, and the ratio of optical to electronic gain of the two channels is 0.998. Using equation (20), a value *R*=0.0109 is obtained. Because the linear polarization degree of the laser is very high, it can be considered that the backscattered
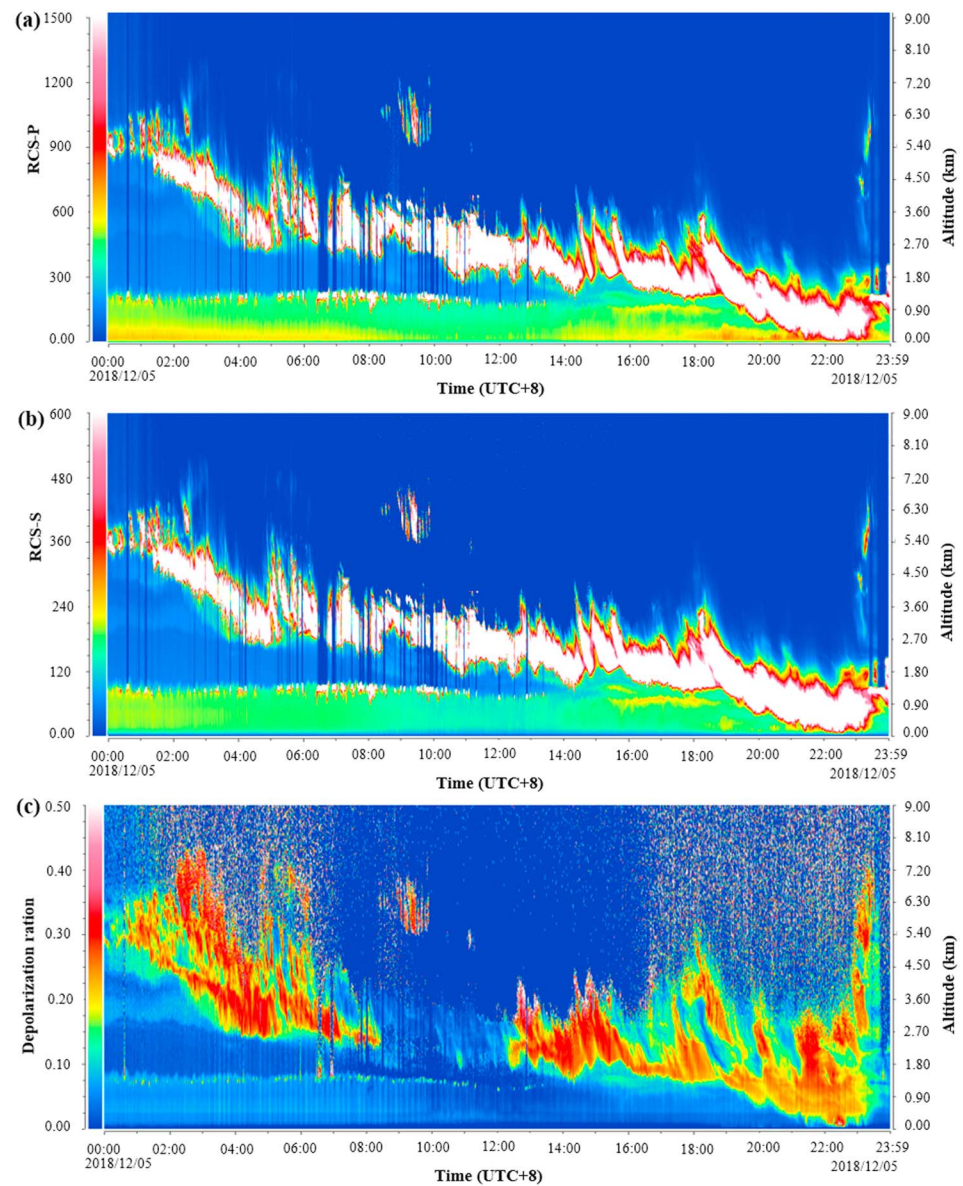
Figure 7. Time-height cross sections of (a) *RCS-P*, (b) *RCS-S*, and (c) depolarization ratio obtained from the proposed algorithm for the lidar data acquired at the Yantai station on 5 December 2018.

power of *RCS-S* is caused by the imperfect parallel alignment between the polarization direction of the laser and the polarization direction of the detector. The depolarization ratio is obtained by equations (19) and (5). Figure 4c shows depolarization ratio calculated by the traditional and proposed methods. It can be seen that the inversion results of those two methods are relatively consistent for well-polarized-calibrated lidar with high system polarization degree. Figures 5a–5c depict, respectively, the time-height cross sections of *RCS-P, RCS-S*, and the depolarization ratio yielded from the proposed algorithm for the lidar data measured at Shenzhen between 18 and 19 December 2018. Those graphics demonstrate the very high stability and continuity of results enabled by our algorithm.

The same procedure displayed in Figure 4 is used for the Yantai's polarized lidar, with results shown in Figure 6. In this case, the ratio of the two channels is about 0.369 for altitudes exceeding 7 km. The ratio of optical and electronic gain of two channels has been measured to be 0.83, and using equation (20), $R=0.306$ is obtained. It can be concluded that this part of the backscattered power is caused by the low system polarization degree. Similar to the Shenzhen site, the depolarization ratio is calculated by

equations (19) and (5). Figure 7 displays the same cross sections as Figure 5, but for the Yantai lidar data measured on 5 December 2018. Similar to the Shenzhen case, the algorithm yields very high stability and continuity (Figure 7). Although the Yantai's lidar system polarization degree is relatively low, the depolarization ratio can still be calculated by the proposed algorithm.

5. Conclusions

An algorithm was proposed to retrieve the depolarization ratio from polarization lidar data. Results from numerical simulations showed a good agreement between the simulated depolarization ratio profile and the one obtained from the proposed algorithm, while experimental results demonstrated that the proposed algorithm yields very high stability and accuracy. Thus, the proposed algorithm no longer requires the laser source to be linearly polarized, allowing for elliptical or random polarization (except circular) to be used. During the installation process, the polarization of the detector is no longer required to be parallel or perpendicular to the polarization plane of the laser source and can be done in any direction.

References

Ansmann, A., Bösenberg, J., Chaikovsky, A., Comeron, A., Eckhardt, S., Eixman, R., et al. (2003). Long range transport of Saharan dust to northern Europe: the 11–16 October 2001 ourtbreak observed with EARLINET. *Journal of Geophysical Research*, *108*(D24), 4783. https://doi.org/10.1029/2003JD003757

Behrendt, A., & Nakamura, T. (2002). Calculation of the calibration constant of polarization lidar and its dependency on atmospheric temperature. *Optics Express*, *10*(16), 805–817. https://doi.org/10.1364/OE.10.000805

Belegante, L., Bravo-Aranda, J. A., Freudenthaler, V., Nicolae, D., Nemuc, A., Ene, D., et al. (2018). Experimental techniques for the calibration of lidar depolarization channels in EARLINET. *Atmospheric Measurement Techniques*, *11*, 1119–1141. https://doi.org/10.5194/amt-11-1119-2018

Bockmann, C., Wandinger, U., Ansmann, A., Bosenberg, J., Amiridis, V., Boselli, A., et al. (2004). Aerosol lidar intercomparison in the frame-work of the EARLINET project. 2. Aerosol backscatter algorithms. *Applied Optics*, *43*, 977–989. https://doi.org/10.1364/AO.43.000977

Bravo-Aranda, J. A., Belegante, L., Freudenthaler, V., Alados-Arboledas, L., Nicolae, D., Granados-Muñoz, M. J., et al. (2016). Assessment of lidar depolarization uncertainty by means of a polarimetric lidar simulator. *Atmospheric Measurement Techniques*, *9*, 4935–4953. https://doi.org/10.5194/amt-9-4935-2016

Browell, E. V., Butler, C. F., Ismail, S., Robinette, P. A., Carter, A. F., Higdon, N. S., et al. (1990). Airborne lidar observations in the wintertime Arctic stratosphere: Polar stratosphere clouds. *Geophysical Research Letters*, *17*, 385–388. https://doi.org/10.1029/GL017i004p00385

Freudenthaler, V. (2016). About the effects of polarising optics on lidar signals and the Δ90 calibration. *Atmospheric Measurement Techniques*, *9*, 4181–4255. https://doi.org/10.5194/amt-9-4181-2016

Freudenthaler, V., Esselborn, M., Wiegner, M., Heese, B., Tesche, M., Ansmann, A., et al. (2009). Depolarization ratio profiling at several wavelengths in pure Saharan dust during SAMUM 2006. *Tellus*, *61B*, 165–179. https://doi.org/10.1111/j.1600-0889.2008.00396.x

Klett, J. D. (1981). Stable analytical inversion solution for processing lidar returns. *Applied Optics*, *20*, 211–220. https://doi.org/10.1364/AO.20.000211

Mamouri, R. E., Ansmann, A., Nisantzi, A., Kokkalis, P., Schwarz, A., & Hadjimitsis, D. (2013). Low Arabian extinction-to-backscatter ratio. *Geophysical Research Letters*, *40*, 4762–4766. https://doi.org/10.1002/grl.50898

Murayama, T., Okamoto, H., Kaneyasu, N., Kamataki, H., & Miura, K. (1999). Application of lidar depolarization measurement in the atmospheric boundary layer: effects of dust and sea-salt particles. *Journal of Geophysical Research*, *104*, 31,781–31,792. https://doi.org/10.1029/1999jd900503

Platt, C. M. R., Scott, C., & Dilley, A. D. (1987). Remote sounding of high clouds. Part IV: Optical properties of midlatitude and tropical cirrus. *Journal of the Atmospheric Sciences*, *44*, 729–747. https://doi.org/10.1175/1520-0469(1987)0442.0.CO;2,1987

Sassen, K. (1991). The polarization lidar technique for cloud research: A review and current assessment. *Bulletin of the American Meteorological Society*, *72*, 1848–1866. https://doi.org/10.1175/1520-0477(1991)072<1848:TPLTFC>2.0.CO;2

Sassen, K., Griffin, M. K., & Dodd, G. C. (1989). Optical scattering and microphysical properties of subvisual cirrus clouds and climatic implications. *Journal of Applied Meteorology*, *28*, 91–91. https://doi.org/10.1175/1520-0450(1989)028<0091:OSAMPO>2.0.CO;2

Scotland, R. M., Sassen, K. R., & Stone, J. (1971). Observations by lidar of linear depolarization ratios by hydrometeors. *Journal of Applied Meteorology*, *10*, 1011–1017. https://doi.org/10.1175/1520-0450(1971)0102.0.CO;2

Shimizu, A., Sugimoto, N., Matsui, I., Arao, K., Uno, I., Mu-rayama, T., et al. (2004). Continuous observations of Asian dust and other aerosols by polarization lidar in China and Japan during ACE-Asia. *Journal of Geophysical Research*, *109*, D19S17. https://doi.org/10.1029/2002JD003253

Sugimoto, N., & Lee, C. H. (2006). Characteristics of dust aerosols inferred from lidar depolarization measurements at two wavelengths. *Applied Optics*, *45*, 7468–7474. https://doi.org/10.1364/AO.45.007468

Xian, J., Han, Y., Huang, S., Sun, D., Zheng, J., Han, F., et al. (2018). Novel Lidar algorithm for horizontal visibility measurement and sea fog monitoring. *Optics Express*, *26*, 34,853–34,863. https://doi.org/10.1364/OE.26.034853